ADVANCES IN ATMOSPHERIC SCIENCES, VOL. 30, NO. 3, 2013, 855–867

Evaluation of Grid-point Atmospheric Model of IAP LASG Version 2 (GAMIL2)

LI Lijuan*[1] (李立娟), WANG Bin[1,2] (王 斌), DONG Li[1] (董 理), LIU Li[2] (刘 利), SHEN Si[1] (申 思), HU Ning[1] (胡 宁), SUN Wenqi[1] (孙文奇), WANG Yong[1] (王 勇), HUANG Wenyu[2] (黄文誉), SHI Xiangjun[3] (史湘军), PU Ye[1] (普 业), and YANG Guangwen[2] (杨广文)

[1]*State Key Laboratory of Numerical Modeling for Atmospheric Sciences and Geophysical Fluid Dynamics, Institute of Atmospheric Physics, Chinese Academy of Sciences, Beijing* 100029

[2]*Ministry of Education Key Laboratory for Earth System Modeling, Center of Earth System Science, Tsinghua University, Beijing* 100084

[3]*Climate Center, Hebei Meteorological Administration, Shijiazhuang* 050021

(Received 20 July 2012; revised 16 December 2012)

ABSTRACT

The Grid-point Atmospheric Model of IAP LASG version 2 (GAMIL2) has been developed through upgrading the deep convection parameterization, cumulus cloud fraction and two-moment cloud microphysical scheme, as well as changing some of the large uncertain parameters. In this paper, its performance is evaluated, and the results suggest that there are some significant improvements in GAMIL2 compared to the previous version GAMIL1, for example, the components of the energy budget at the top of atmosphere (TOA) and surface; the geographic distribution of shortwave cloud radiative forcing (SWCF); the ratio of stratiform versus total rainfall; the response of atmospheric circulation to the tropical ocean; and the eastward propagation and spatiotemporal structures of the Madden Julian Oscillation (MJO). Furthermore, the indirect aerosols effect (IAE) is -0.94 W m^{-2}, within the range of 0 to -2 W m^{-2} given by the IPCC 4th Assessment Report (2007). The influence of uncertain parameters on the MJO and radiation fluxes is also discussed.

Key words: GAMIL, Madden Julian Oscillation, SWCF, indirect aerosol effectw

Citation: Li, L. J., and Coauthors, 2013: Evaluation of Grid-point Atmospheric Model of IAP LASG version 2 (GAMIL2). *Adv. Atmos. Sci.*, **30**(3), 855–867, doi: 10.1007/s00376-013-2157-5.

1. Introduction

The Grid-point Atmospheric Model of IAP LASG (GAMIL) is an AGCM based on a finite difference dynamical core and developed by the State Key Laboratory for Numerical Modeling of Atmospheric Sciences and Geophysical Fluid Dynamics (LASG), Institute of Atmospheric Physics (IAP), Chinese Academy of Sciences (CAS). Its horizontal grids consist of a uniform zonal grid (the grid interval is 2.8°) and a hybrid meridional grid with the Gaussian grid in the zone between 65.58°S and 65.58°N (the grid length is about 2.8°) and a weighted even-area grid in the high latitudes and polar region (the grid size is generally larger than 2.8°). The model includes 26-σ vertical levels (pressure normalized by surface pressure) with the model top at 2.194 hPa. Owing to the use of a weighted even-area grid in the high latitudes, the dynamical core is computationally highly stable without any filtering or smoothing in the polar region. In particular, some important integral properties are conserved exactly, such as the antisymmetries of the horizontal and vertical advection operator, the mass conservation, and the effective total energy conservation under the standard stratification approximation. For details about the dynamical core, please refer to Wang

*Corresponding author: LI Lijuan, ljli@mail.iap.ac.cn

et al. (2004) and Wang and Ji (2006).

The physical processes in its first version, GAMIL1, mainly come from the Community Atmospheric Model (CAM2) (Collins et al., 2003), but for another convective scheme (Tiedtke, 1989; Nordeng, 1994; Li et al., 2007a) and some changed parameters for the energy balance at the top of atmosphere (TOA) and the surface, such as the liquid water path (LWP) (Li et al., 2008).

GAMIL has taken part in various international model intercomparison projects, such as the Atmospheric Model Intercomparison Project (AMIP), Climate of the 20th Century (C20C), Climate Prediction and its Societal Application (CliPas), and Cloud Feedback Model Intercomparsions Project Phase II (CFMIP II), and has been widely used in studies of 20th century climate change, seasonal prediction, variability of the Asian–Australian monsoon, subtropical high, cloud feedback, Madden-Julian Oscillation (MJO), and Pacific–North America teleconnection (e.g. Li et al., 2007b, c; Wu and Li, 2008; Kuang et al., 2009; Kucharski et al., 2009; Scaife et al., 2008; Zou et al., 2009; Hodson et al., 2010; Li and Wang, 2010; Guo et al., 2011; Dong et al., 2012; Li et al., 2012; Mao and Li, 2012; Xie et al., 2012). Moreover, as an atmospheric component of the grid-point version of the Flexible Global Ocean-Atmosphere-Land System model (FGOALS-g), GAMIL has also served as a scientific tool for studying other scientific issues, such as paleoclimate change, ENSO, and tropical biases (Lin, 2007; Yu and Sun, 2009; Zheng and Yu, 2009; Yan et al., 2010).

Through those intercomparisons and applications, a comprehensive picture of the performance of GAMIL has been constructed, highlighting both its skill and deficiencies compared with observations or reanalyses. Such work is the foundation for its ongoing development. For instance, some studies have indicated that GAMIL reproduces wind rotation styles and wind onset reasonably well over most monsoon regions (Zhang and Li, 2007; Li and Zhang, 2009), and GAMIL one-month lead prediction is basically able to capture the major patterns of the long-term annual mean as well as the first annual cycle mode (Wu and Li, 2009). Other studies, however, have suggested that the tropical response of GAMIL to specified SST is obviously weaker than that of the National Centre for Environmental Prediction (NCEP) Reanalysis (Scaife et al., 2008; Yu and Sun, 2009), and there are obvious biases in the simulations of cloud radiative forcing (CRF) by GAMIL and other climate models (Guo et al., 2011). Alleviating those biases will be one of the most important objectives for the next version of GAMIL.

The rest of the paper is organized as follows. Section 2 describes the major changes in GAMIL2 compared with its previous version. The experiment design and observational data for model validation are introduced in section 3. Section 4 presents the results from GAMIL2 simulations including climate mean states, MJO and the aerosols indirect effect (AIE). Section 5 provides a summary and conclusions.

2. Major changes in GAMIL2

Compared with its previous version (GAMIL1), the major changes in GAMIL2 are the upgrade of cloud-related processes (see Table 1) and the resetting of some uncertain parameters in shallow and deep convection schemes, as well as the cloud fraction, cloud microphysical processes and boundary layer schemes (Table 2). Most of these parameter values are reset in the FGOALS-g2 framework according to its performance in terms of the long-term stabilities, atmospheric climate mean state, ENSO) (e.g. the standard deviation of the Niño3 index), and evolutions of 20th century surface temperature simulations etc. in the preindustrial control runs and historical runs (Li et al., 2013), except for the energy balance of TOA (or model) in the AMIP runs. The influence of uncertain parameters on climate sensitivity and cloud feedback still is a hot topic, and has been explored in other climate models such as the Hadley Centre Atmospheric Model with slab ocean (HadSM), the Model for Interdisciplinary Research on Climate (MIROC), and the Community Atmospheric Model (CAM) (Stainforth et al., 2005; Jackson et al., 2008; Yokohata et al., 2010; Sanderson, 2011). In this study, only the results of the tuned parameters are given, and their effects on model performance will be discussed in another study.

GAMIL2 uses the deep convective parameterization scheme by Zhang and Mu (2005), a revised Zhang and McFarlane (1995) version with three modifications (Table 1). They are the quasi-equilibrium type closure assuming that a quasi equilibrium exists between

Table 1. Major difference between the physical schemes of GAMIL1 and GAMIL2.

	GAMIL1	GAMIL2
Deep convection parameterization	Zhang and McFarlane (1995)	Zhang and Mu (2005)
Convective cloud fraction	Rasch and Kristjánsson (1998)	Xu and Krueger (1991)
Cloud microphysical scheme	Rasch and Kristjánsson (1998)	Morrison and Gettleman (2008)

Table 2. Mainly reset parameters in GAMIL2.

Parameters	Description	Original values	New values
c0	rain water autoconversion coefficient for deep convection	$2.\times10^{-3}$	$5.\times10^{-4}$
ke	evaporation efficiency for deep convection	7.5×10^{-6}	9.0×10^{-6}
rhcrit	threshold value for rh for deep convection	0.8	0.9
capelmt	threshold value for cape for deep convection	70	80
rhminl	threshold RH for low clouds	0.93	0.91
rhminh	threshold RH for high clouds	0.8	0.78
c0	rain water autoconversion coefficient for shallow convection	$1.\times10^{-4}$	$5.\times10^{-5}$
cmftau	characteristic adjustment time scale of shallow cape	3600.	7200.
wsub	sub-grid vertical velocity for aerosol activation	wsub=max(0.1,wsub)	wsub=max(0.5,wsub)
kvm	diffusion coefficient for momentum	no minum limitation	kvm=max(5.0,kvm)
kvh	diffusion coefficient for heat	No minum limitation	kvh=max(1.0,kvh)
conke	rate of evaporation of stratiform precipitation	$1.\times10^{-5}$	$5.\times10^{-6}$
icritic	threshold for autoconversion of cold ice	$6.\times10^{-6}$	$5.\times10^{-6}$
icritw	threshold for autoconversion of warm ice	$5.\times10^{-4}$	$4.\times10^{-4}$

convection and large-scale processes in the free troposphere, including a relative humidity (RH) threshold as a convection trigger to suppress convection in the excessively dry boundary layer and removing the restriction that convection only originates from the layers below the Planetary Boundary Layer (PBL) top. Furthermore, uncertain parameters in the convection scheme have been updated regarding the overestimation of deep convection precipitation and its occurrence, such as the rain water auto-conversion coefficient (c0), the evaporation efficiency (ke), the threshold value for cape (capelmt), and the threshold value of RH (rhcrit) for deep convection, and the characteristic adjustment time scale (cmftau) and rain water autoconversion coefficient (c0) for the Hack (1994) shallow convection (Table 2).

There are three types of clouds, all of which are estimated using the diagnostic Slingo-type scheme. The convective clouds are related to updraft mass flux (a direct measure of the convection intensity) in the deep and shallow cumulus schemes according to a functional form suggested by Xu et al. (1991). The Marine stratocumulus clouds are diagnosed by the lower-tropospheric stability defined by the potential temperature difference between 700 hPa and the surface (Klein et al., 1993). Furthermore, the layered clouds are calculated according to RH (Collins et al., 2004). The parameters, such as rhminl (threshold RH for low clouds), rhminh (threshold RH for high clouds), have been adjusted for the energy balance and better CRF simulations (Table 2).

The two-moment scheme, including both number concentration (NC) and mass mixing ratio (MMR) of cloud particles, proposed by Morrison and Gettelman (2008), was transplanted into GAMIL2 by Shi et al. (2010) to represent microphysical processes. The precipitation MMRs and NCs are diagnosed, while the cloud droplet and cloud ice MMRs and NCs are predicted. There are two choices for the aerosol activation: Abdul-Razzak and Ghan (2000) and Nenes and Seinfeld (2003). Only the former is used in this study. For reasonable 20th century global warming to be simulated by FGOALS-g2, some parameters and thresholds affecting the aerosol activation have been modified; for instance, the sub-grid vertical velocity (wsub) minimum value. Moreover, the parameters in the macrophysics and boundary layer schemes have been trained corresponding to the parameter changes in other processes (Table 2).

3. Experiment design and observational data

Two sets of numerical experiments are performed following the standard settings for Phase II of the Atmospheric Model Intercomparison Project (AMIP II). One simulation covered the period 1979–2008, forced by the time-varying solar constant, greenhouse gases (GHGs), aerosols (including sulphate, black and organic carbon, dust, and sea salt), ozone, and Hadley Centre Sea Ice and Sea Surface Temperature data (HadISST), for the model climatological mean and variability analyses. The solar constant was the annually resolved total solar irradiation (TSI) with the background recommended by the CMIP5 (Lean, 2009). Concentrations of greenhouse gases were specified by the IIASA (International Institute for Applied Systems Analysis) website: http://www.iiasa.ac.at/webapps/tnt/RcpDb/dsd?Action=htmlpage&page=welcome. The AC&C (Atmospheric Chemistry & Climate)/SPARC (Stratospheric Processes and their Role in Climate) ozone database was used for ozone forcing, which consists of separate

stratospheric and tropospheric data sources (Cionni et al., 2011). The aerosol files were monthly 10-year averages centered around the middle of each decade produced by the Community Atmospheric Model, version 3.5 (CAM3.5), with a bulk aerosol model recommended by the CMIP5, and linearly interpolated in time from year to year within each month. Another set of two simulations were run for five years forced by present day (PD; the year 1995) and preindustrial (PI; the year 1850) aerosols respectively, with other annual cycle/fixed forcings the same (e.g. annual cycle SST, fixed GHGs and solar constant), for the indirect aerosol effect (IAE). That is, the only difference between the PD and PI simulation was the aerosol forcing.

For model validation, datasets from the Clouds and the Earth's Radiant Energy System (CERES) - Energy Balanced and Filled (EBAF) (from March 2000 to February 2010), the International Satellite Cloud Climatology Project - Flux Data (ISCCP-FD), the National Oceanic and Atmospheric Administration (NOAA), the NCEP Reanalysis II, and the European Centre for Medium-Range Weather Forecasts (ECMWF) Reanalysis were used.

4. Results

4.1 *Climatological mean state*

Accurate simulation of the radiation energy budget is one of the most important properties of an AGCM as the distribution of incoming and outgoing radiative energy fluxes is the primary forcing agent for the general circulation of the atmosphere. Table 3 presents globally averaged annual mean components of the energy budget at the TOA and surface by GAMIL2 and ISCCP-FD during the different periods and the recent estimation by Trenberth et al. (2009) (TFK09) from March 2000 to May 2004 based on updated observation datasets [including improvements in retrieval methodology and hardware compared with those in Kiehl and Trenberth (1997) (KT97), e.g. a uniform albedo scaling rather than the direct ASR scaling as in KT97, and the incorporation of CERES] and radiative transfer models. Firstly, we note that there are large uncertainties between the observations and TFK09, even for the same ISCCP-FD observation at different times. In particular, the difference of the Absorbed Shortwave Radiation (ASR) is closely related to the solar radiation reflected by the atmosphere. Furthermore, the Outgoing Longwave Radiation (OLR) at the TOA between the observations and estimation of TFK09 exceeds 3 W m^{-2}, which is very close to the radiative forcing ($\sim$3.7 W m^{-2}) due to doubled CO_2 in the IPCC 3rd Assessment Report (2001). Secondly, the radiation fluxes at the TOA and surface are reasonably reproduced by GAMIL2, except for the higher longwave radiation up at the surface, which could attribute to both the higher land skin temperature (data not shown) and different temporal scales compared with the observations and estimates (Trenberth et al., 2009). Also, the influence of temporal coverage is not neglected, e.g. for the simulation period from January 1979 to December 2008, for March 2000 to May 2004 in TKF09 and ISCCP-FD R, and for February 1985 to

Table 3. TOA and surface globally-averaged annual mean radiation budget. TKF09 refers to Trenberth et al. (2009); and ISCCP-FD R and ISCCP-FD B refer to the periods of Mar 2000 to May 2004 and Feb 1985 to Apr 1989 respectively. The units are W m^{-2} for all of the variables except for albedo (%).

Global	GAMIL2	TFK09	ISCCP-FD R	ISCCP-FD B
TOA radiation budget				
Solar in	341.6	341.3	341.7	341.8
Solar reflected	103.7	101.9	105.2	105.9
ASR	237.9	239.4	236.5	235.8
Albedo	32.0	29.8	30.8	31.0
OLR	238.9	238.5	235.6	233.3
Net down at TOA	−1.0	0.9	0.9	2.5
Surface radiation budget				
Solar reflected	24.3	23.1	22.8	24.0
Solar absorbed	70.3	78.2	70.8	70.9
Net Solar down	167.6	161.2	165.7	164.9
LH	84.3	80.0	—	—
SH	20.1	17	—	—
LW Radiation up	401.3	396	393.9	395.5
Back LW Radiation	336.3	333	345.4	344.8
Net LW	65.0	63	48.5	51.0
Net down at surface	−1.8	0.9	—	—

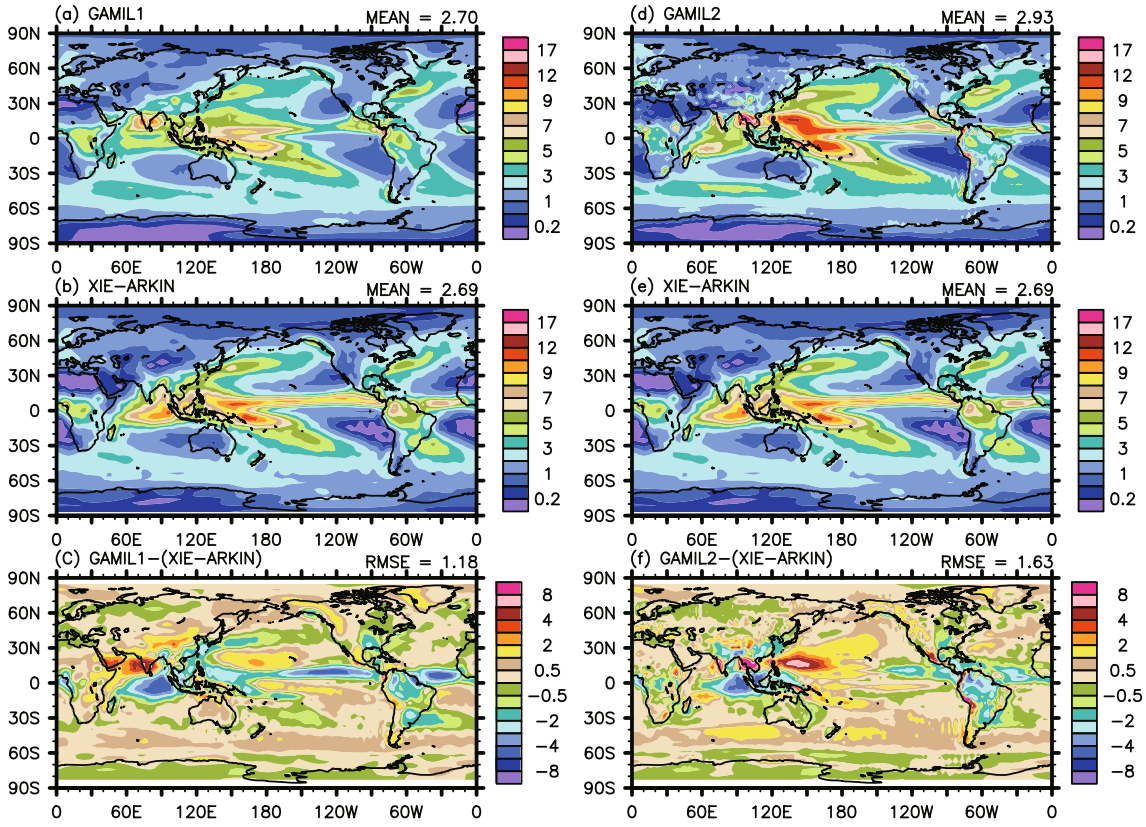

Fig. 1. Annual mean rainfall from GAMIL simulations, Xie-Arkin observations and their differences. MEAN represents the global mean value. Units: mm d^{-1}.

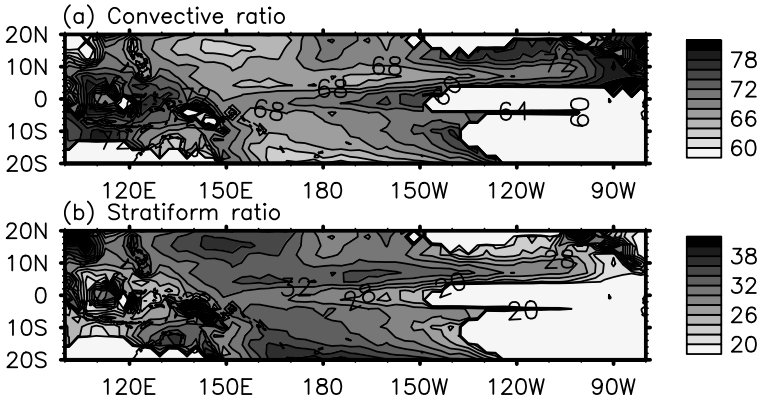

Fig. 2. Fraction of annual mean (a) convective and (b) stratiform precipitation by GAMIL2 in the tropical Pacific region. Areas with less than 0.6 m yr^{-1} annual average rainfall are not included.

April 1989 in ISCCP-FD B. Thirdly, the energy residual is −1.0 and −1.8 W m^{-2} at the TOA and surface respectively, which means there is 0.8 W m^{-2} resident in the atmosphere. About 0.57 W m^{-2} is from the imbalance (∼0.02 mm d^{-1}) between the evaporation and precipitation resulting from non-conservative water vapor advection, whereas the remainder could be associated with the given increase of the GHG mixing ratio and SST during the past 30 years, resulting in more longwave fluxes in the atmosphere.

The annual mean total rainfall and convective/stratiform ratios in the total precipitation are shown in Figs. 1 and 2. Overall, the global mean (Fig. 1d) and RMSE (Fig. 1f) of precipitation simulated by GAMIL2 are larger than those by GAMIL1 (Figs. 1a and f). GAMIL2 produces more rainfall over the Indo-China Penisula, South China Sea, Philippine Sea, and westerly wind belt in the SH than Xie-Arkin (Figs. 1b and e) as well as GAMIL1. Meanwhile, the negative biases over the ITCZ, South Pacific Conver-

gence Zone (SPCZ) and sub-tropical monsoon region (east of Japan) in GAMIL1 are largely decreased in GAMIL2. Particularly the grid-resolved precipitation ratio in the tropical Pacific in the new version is nearly 30% of the total (Fig. 2), higher than the 10%–20% for the previous version (Li et al., 2007a), and thus influences the MJO through changed heating profiles (Fu and Wang, 2009). Another noticeable feature is that the global mean rainfall strength is different from that reported by Xie et al. (2012), although their spatial patterns were similar. This is due to some different parameter values in the moist processes in the model (e.g. c0, ke, rhminl, and rhminh; Table 2).

The biases of the shortwave/longwave cloud forcing (SWCF/LWCF) geographic distribution in GAMIL2 are reduced, especially in the central tropical Pacific and northern-western Indian Ocean (Figs. 3 and 4). The global mean values simulated by GAMIL2 are closer to the CERES-EBAF observations and the RMSEs are smaller than those produced by GAMIL1. This improvement is consistent with its better simulations of cloud (Dong et al., 2012) and liquid water path (figure not shown). All of these are further connected with the updated cloud macro-/microphysics schemes and their coordination with other schemes, such as convection.

The vertical distributions of the zonal mean temperature and zonal wind are captured by GAMIL2 (Fig. 5). In particular, the temperature differences between the simulation and observation in the troposphere are less than 4°C and the results using the Tiedtke (1989) convection parameterization (Fig. 4 in Li et al., 2007a), indicating the effects of the convective scheme on the heating profile. Also, the cold biases between 100 hPa and 50 hPa are significantly alleviated, perhaps related to the time-varying stratospheric ozone, though the large biases of the temperature and zonal wind still exist in the stratosphere. In accordance with the improvement of SWCF/LWCF, rainfall and temperature in the tropical region, the biases of zonally averaged zonal wind are less than 3 m s^{-1} in the troposphere and smaller than 6 m s^{-1} in GAMIL1 (figure not shown). Whereas, the west winds in the Southern Ocean region (45°–60°S) shift northward and become weak compared with the reanalysis as, well as GAMIL1 (figure not shown).

The regression coefficient between the Southern Oscillation Index (SOI) and Niño3 was used to compare the strength of the atmospheric response to the tropical Pacific Ocean in GAMIL1, GAMIL2 and the

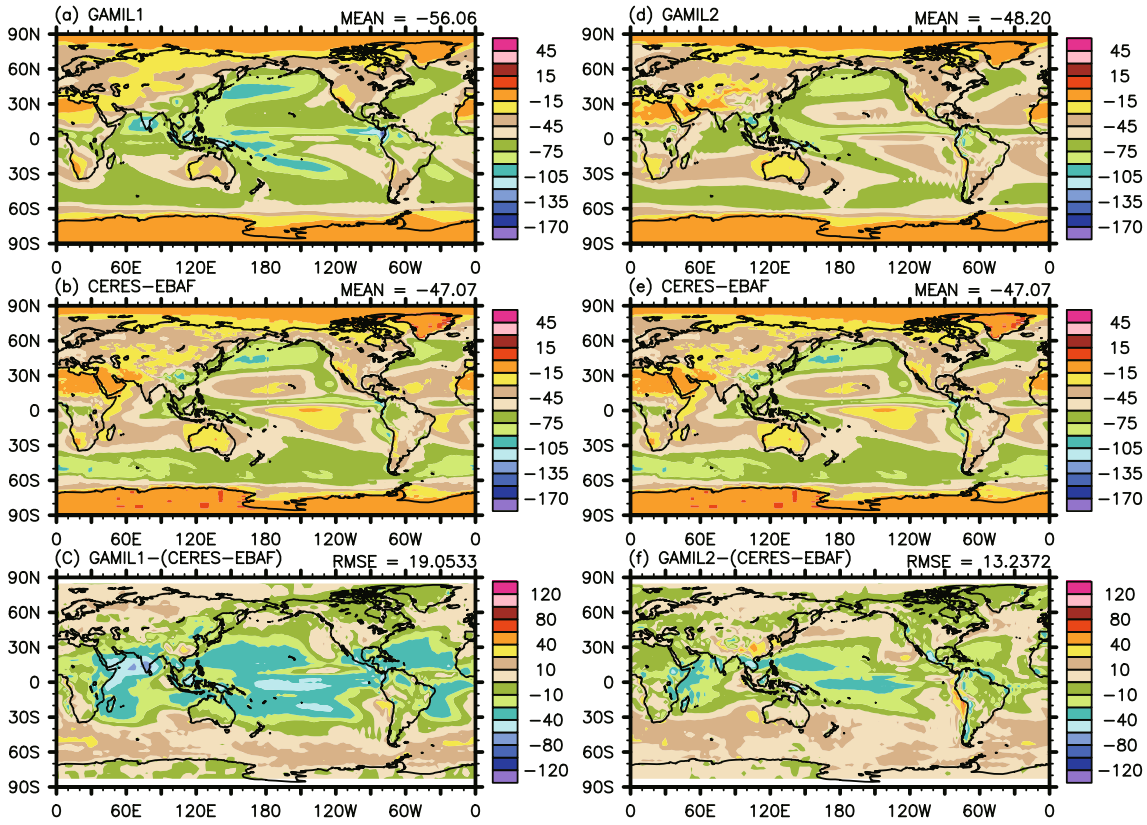

Fig. 3. The same as Fig. 1 but for SWCF. Units: W m^{-2}.

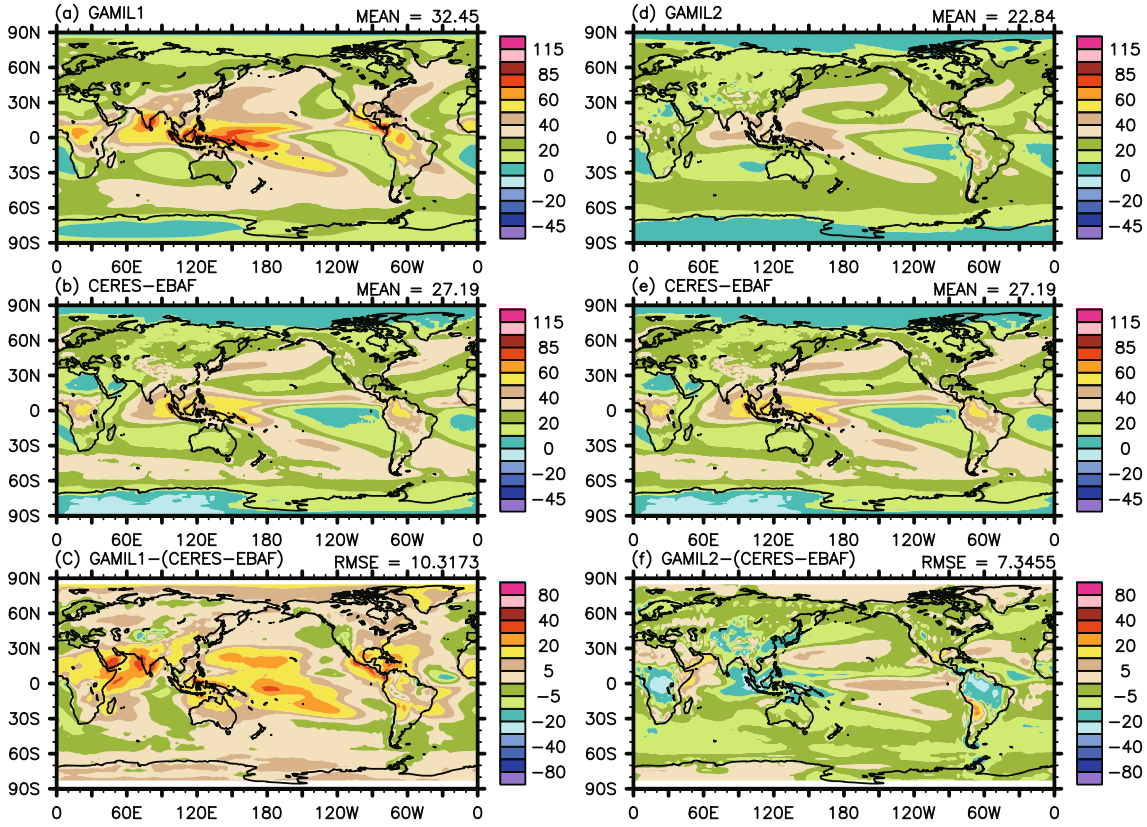

Fig. 4. The same as Fig. 3 but for LWCF.

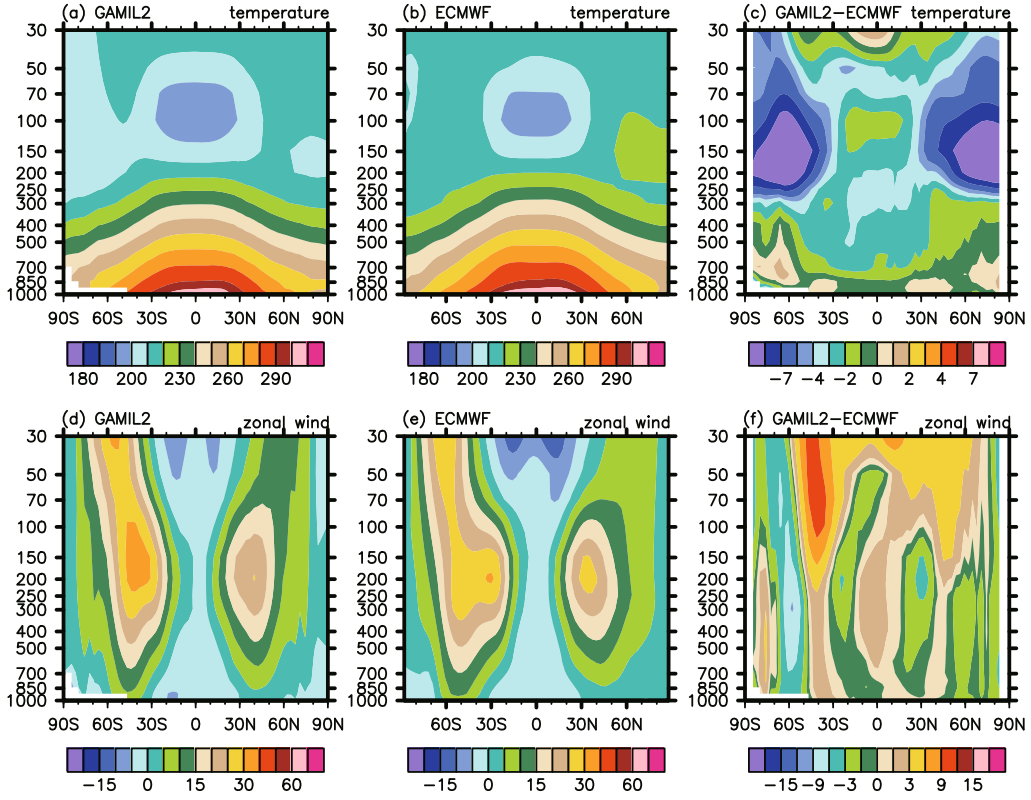

Fig. 5. Vertical profiles of zonal mean temperature (°C) and zonal wind ($m\ s^{-1}$) for (a, d) GAMIL2, (b, e) ECMWF and (c, f) their differences.

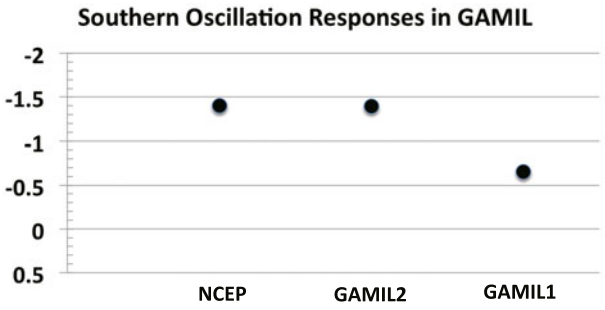

Fig. 6. Regression coefficients between the SOI and Niño3. Here, SOI is defined as the difference between Tahiti and Darwind pressure. Units: hPa $°C^{-1}$.

NCEP Reanalysis II according to Scaife et al. (2008), the results of which are shown in Fig. 6. Significant improvement can be sighted in GAMIL2, which presents a coefficient much closer to that of NCEP than GAMIL1 [GAMIL1.1 used in Scaife et al. (2008)]. The reason for this could be related to the artificially amplified LWP in GAMIL1 and 1.1 for the energy balance at the TOA, which is enlarged spuriously from the global mean 70 g m^{-2} to 110 g m^{-2} in both versions, and then results in a false response of the SWCF and other corresponding variables to the tropical Pacific.

4.2 *MJO*

Figure 7 shows the lag-longitude and -latitude diagrams of intraseasonal OLR (shaded) and 850-hPa zonal wind (contour) within the reference area (from 10°S to 5°N, and from 75°E to 100°E) in boreal winter. Some important characteristics are better simulated by GAMIL2 than by GAMIL1, such as the confinement of the convection to the Eastern Hemisphere, faster eastward propagation in the Western Hemisphere, lag relationship between the OLR and zonal wind, only with weak amplitude [also seen in Xie et al. (2012)]. However, for the northward propagation, no significant signal is captured in the simulation, while a weak one is present in Xie et al. (2012). The difference between the two studies is some large uncertainties in parameters (such as c0, ke, and rhminl) in the moist processes, suggesting their important influence on the MJO northward propagation.

The first two modes of multivariate EOF (MEOF)

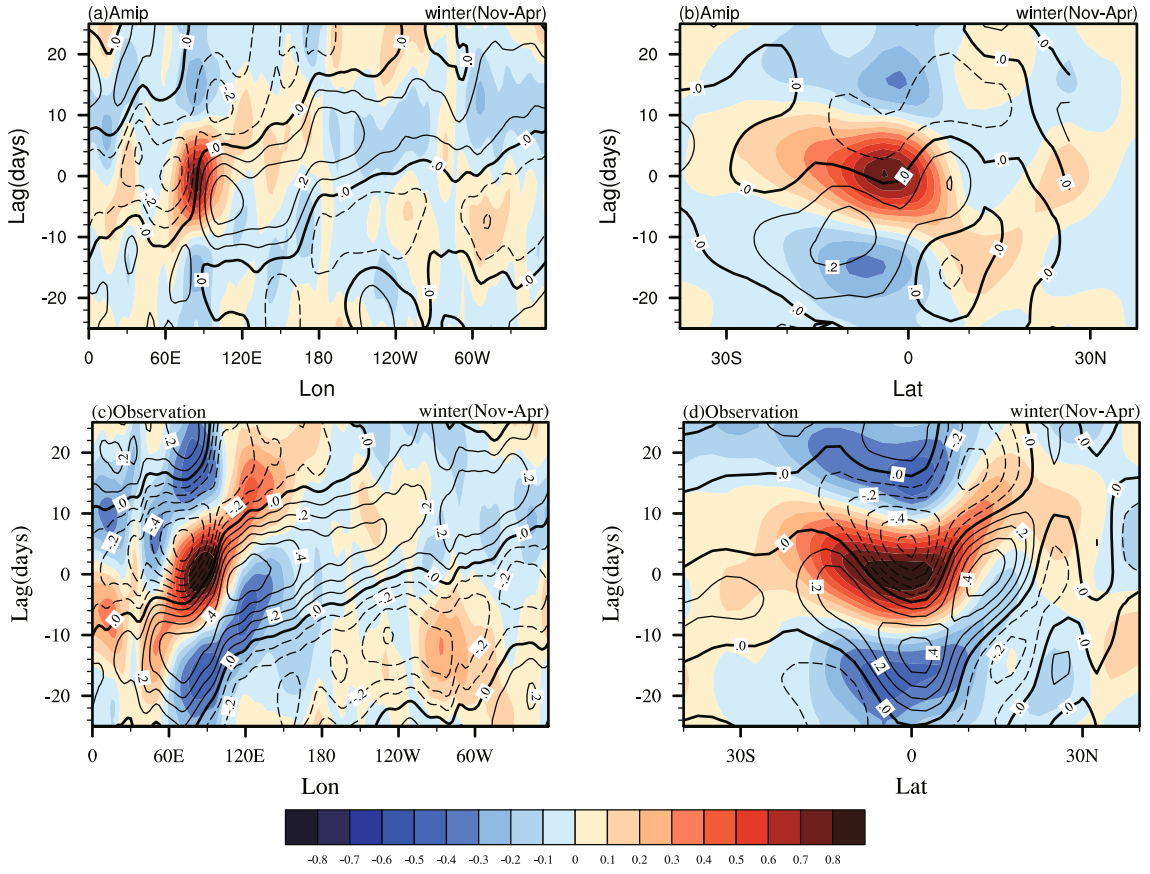

Fig. 7. Simulated (a, b) and observed (c, d) lag-regression zonal mean (80°–100°E) and meridional mean (10°S–10°N) of U850 (contour 0.1 intervals, m s^{-1}) and OLR (shaded, W m^{-2}) upon the spatial average OLR within the reference area (10°S–5°N, 75°–100°E) in winter.

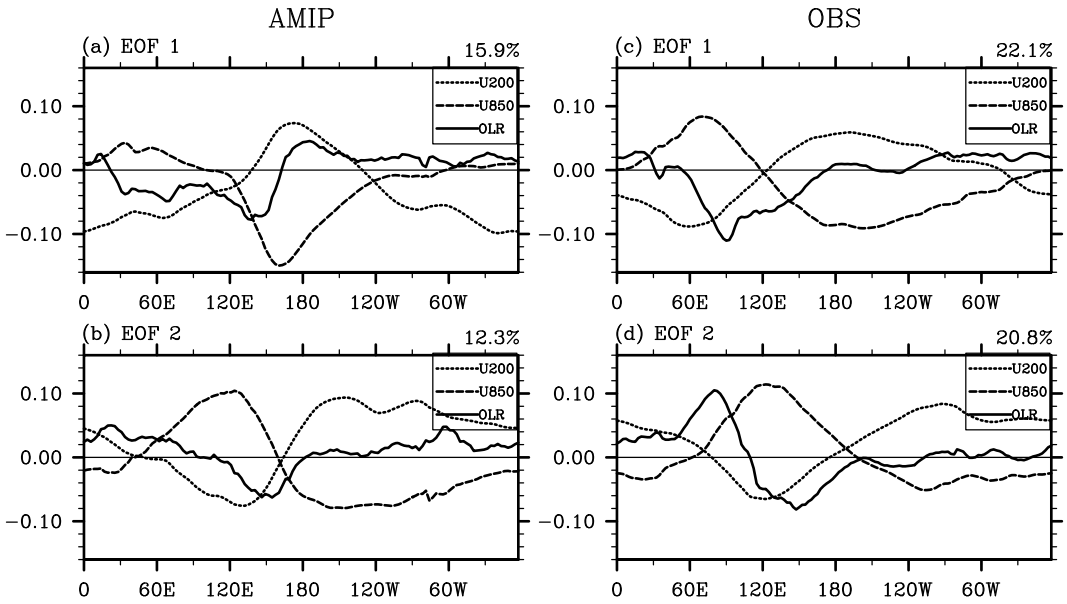

Fig. 8. Multivariate combined EOF analysis of meridional mean U200, U850 and OLR. (15°S–15°N) from the (a, b) simulation and (c, d) observation. All results were converted to anomalies with a 20–100-day bandpass-filter before they were analyzed.

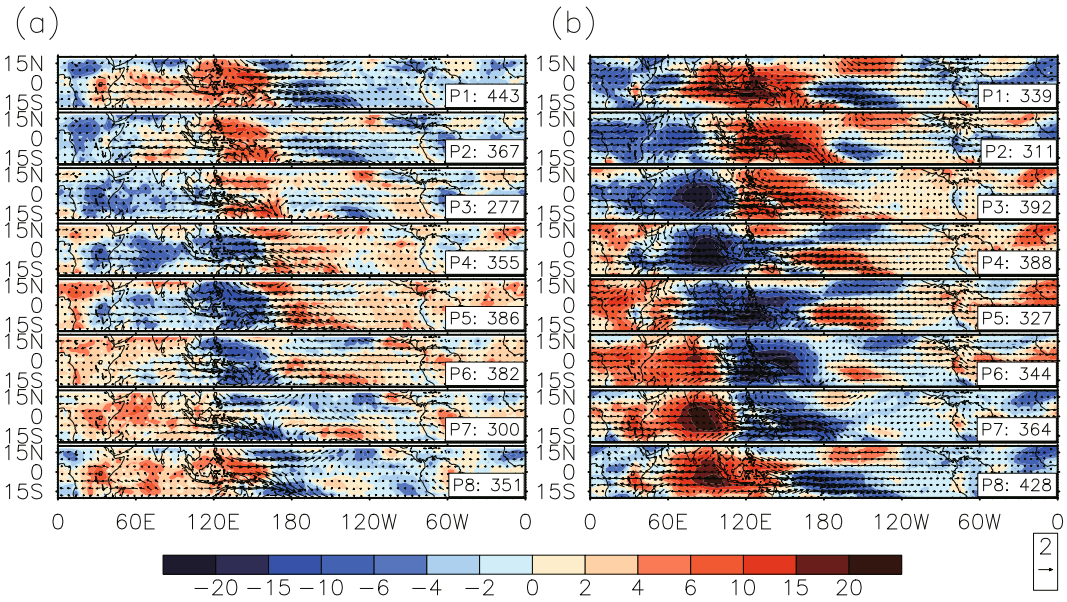

Fig. 9. MJO composite of OLR (shaded W m^{-2}) and 850-hPa wind (vector) in eight phases from November to April for (a) GAMIL and (b) observation.

analysis of the NCEP Reanalysis and simulation are depicted in Fig. 8. GAMIL2 reasonably reproduces the coupled convection and wind structure as that in the observation in spite of the weak convection strength in the first mode, which is also found in Xie et al. (2012). The ratios of variance contribution of the two modes by GAMIL2 are 15.9% and 12.3% respectively, less than the 22.1% and 20.8% by NCEP and slightly different from the 15.6% and 13.3% in Xie et al. (2012). Comparing the first mode ratio of 15.9% from GAMIL2 with the 12.3% from FGOALS-g2 (Li et al., 2013), the coupled or uncoupled relationship with the ocean seriously affects the MJO spatial structure. However, the OLR eastward shift from the first mode to the second in Xie et al. (2012) is not obviously seen in this study, indicating again the impacts of the uncertain parameters. This unobvious eastward propagation is also detected in the MJO temporal structure and life cycle in eight phases (Fig. 9). In the observation, the strong convection activities start from the In-

Table 4. Global, NH and SH annual mean changes of SWCF (W m^{-2}), LWP (g m^{-2}), AWNC ($\times 10^9$ m^{-2}), and AREL (μm) between PD and PI (PD minus PI).

	SWCF (W m^{-2})	LWP (g m^{-2})	AWNC (10^9 m^{-2})	AREL (μm)
Global	−0.94	4.76	3.51	−0.06154917
NH	−1.31	7.46	5.83	−0.09550072
SH	−0.58	2.05	1.18	−0.02759763

dian Ocean and propagate eastward until the date line during the life cycle. However, in this study, the convection strength is weak, despite being a little stronger than that in Xie et al. (2012), and the centers are eastward in phases 4 and 5 resulting in the slow propagation since phase 4. Additionally, the range of the convection spread is more concentrated than that in Xie et al. (2012), coordinated with its stronger strength.

4.3 *IAE*

Table 4 gives the indirect effects of the prescribed aerosols on the SWCF, LWP, column droplet number concentration (AWNC), and average cloud droplet effective radius (AREL), i.e. their differences between PD and PI. The global mean SWCF difference by aerosols is −0.94 W m^{-2}, medium in the range of 0 to −2 W m^{-2} estimated by the IPCC 4th Assessment Report (2007). The cooling effect in the NH is −1.31 W m^{-2}, larger than the −0.58 W m^{-2} in the SH, which is in agreement with the aerosol distribution, such as sulfate aerosol [Fig. 1b in Shi et al. (2010)]. Comparing the sulfate aerosol distributions [Fig. 1a in Shi et al. (2010)], there are somehow shifts from the continents to the maritime regions for the shortwave radiative forcing (Fig. 10a). The LWCF change is smaller than their shortwave effect, with a global mean of 0.07 W m^{-2} (Fig. 10b), related to the non-sensitivity to the cloud droplet size.

The aerosol cooling effect is coincident with the increase of cloud condensation nuclei (CCN), AWNC and LWP, and a decrease of the AREL (Table 4; Fig. 11). The CCN distribution agrees especially well

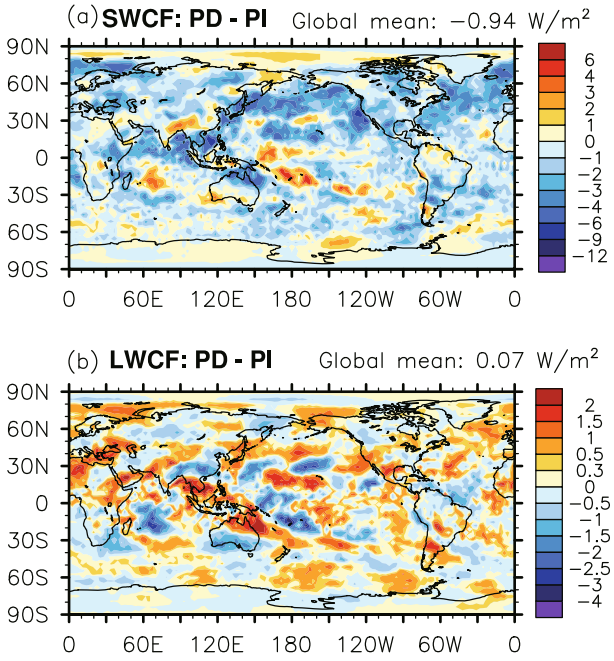

Fig. 10. Geographic distribution of the (a) SWCF and (b) LWCF differences between PD and PI.

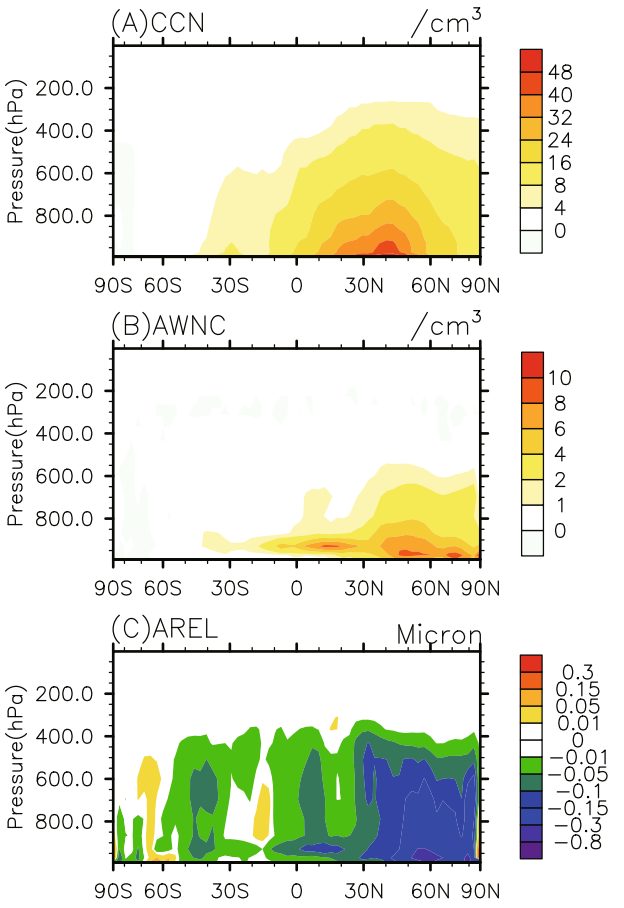

Fig. 11. Vertical profiles of the zonal mean (a) CCN, (b) AWNC and (c) AREL changes from PI to PD (PD minus PI).

with sulfate aerosol, with the maximum between 30°N and 50°N below 800 hPa. The two maximum centers of the CDNC and AREL are located in the regions near 50°N and 10°–20°N, reflecting the impact of the atmospheric circulation on the IAEs.

5. Summary and conclusions

The major changes in GAMIL2 compared with its previous version GAMIL1 have been described. For example, the Zhang and Mu (2005) deep convection scheme has replaced the Zhang and McFarlane (1995) scheme; the Xu et al. (1991) cumulus cloud fraction has taken the place of the Rasch and Kristjánsson (1998) fraction; the two-moment Morrison and Gettelman (2008) cloud microphysical processes are used instead of the one-moment Rasch and Kristjánsson (1998) scheme (Table 1); and the parameters with large uncertainties in the shallow/deep convection, cloud macro-/microphysical processes, and boundary layer schemes have been trained in the FGOALS-g2 framework (Table 2).

The results from the AMIP run by GAMIL2 demonstrate that the components of the energy budgets at the TOA and surface are reasonably reproduced except for the higher longwave radiation up at the surface and 0.8 W m^{-2} resident in the atmosphere. The former could attribute to both the higher land skin temperature and different spatial scales compared to the observations, reanalyses and estimates (Trenberth et al., 2009), and the latter is related to the non-conservative water vapor advection (contributes to about 0.57 W m^{-2}), given the increase of the GHG mixing ratio and SST during the past 30 years resulting in more longwave fluxes in the atmosphere. Also, the geographic distributions of precipitation and SWCF/LWCF and the ratio of stratiform versus total rainfall in the tropical region are significantly improved. Meanwhile, the large biases of rainfall in the tropics and zonal wind in the Southern Ocean region (45°–60°S) are observed. The weak response of the atmosphere to the tropical Pacific Ocean in GAMIL1 is remarkably alleviated in GAMIL2, coming close to that in the NCEP Reanalysis, indicating the coordinated processes and parameters in GAMIL2.

In addition, some important characteristics of the MJO are better simulated by GAMIL2, such as the confinement of the convection to the Eastern Hemisphere, faster eastward propagation in the Western Hemisphere, lag relationship between the OLR and zonal wind, and spatiotemporal structures, only with weak amplitude. However, compared with observations, the eastward propagation is slow and the northward propagation is unobvious. At the same time, we should note there is an influence of the uncertain parameters on MJO northward/eastward propagation and convection strength that cannot be ignored. The detailed mechanism needs to be further studied; for instance, how these parameters affect the heating profile and circulation.

Finally, the IAEs on the SWCF are -0.94 W m^{-2}, -1.31 W m^{-2} and -0.58 W m^{-2} for the globe as a whole, for the NH and for the SH respectively. The cooling effect is coincident with the increase in CCN, AWNC and LWP, as well as the decrease in AREL. Meanwhile, the inconsistency of the geographic distribution of the SWCF, cloud droplet number concentration and sulfate aerosol reflects the impact of the atmospheric circulation.

Acknowledgements. This work was jointly supported by the CAS Strategic Priority Research Program (Grant No. XDA05110304), the National "973" Project (Grant No. 2010CB951904), the China Meteorological Administration R&D Special Fund for Public Welfare (meteorology) (Grant No. GYHY201006014), the National "863" Project (Grant No. 2010AA012304), and the National Natural Science Foundation of China (Grant Nos. 40923002 and 41005053).

REFERENCES

Abdul-Razzak, H., and S. J. Ghan, 2000: A parameterization of aerosol activation 2. Multiple aerosol types, *J. Geophys. Res.,* **105**(D5), 6837–6844.

Cionni, I., and Coauthors, 2011: Ozone database in support of CMIP5 simulations: Results and corresponding radiative forcing. *Atmos. Chem. Phys.*, **11**, 11267–11292, doi: 10.5194/acp-11-11267-2011.

Collins, W. D., and Coauthors, 2003: *Description of the NCAR community atmosphere model* (*CAM2*). National Center for Atmospheric Research, Boulder, CO., 171pp.

Collins, W. D., and Coauthors, 2004: Description of the NCAR Community Atmosphere Model (CAM 3.0). NCAR Tech. Note NCAR/TN-464+STR, NCAR, Boulder, CO., 210pp.

Dong, L., L. J. Li, W. Y. Huang, Y. Wang, and B. Wang, 2012: Preliminary evaluation of the cloud fraction simulations by GAMIL2 using COSP. *Atmos. Oceanic Sci. Lett.*, **5**, 258–263.

Fu, X., and B. Wang, 2009: Critical roles of the stratiform rainfall in sustaining the Madden-Julian oscillation: GCM Experiments, *J. Climate*, **22**, 3939–3959.

Guo, Z., C. Q. Wu, T. J. Zhou, and T. W. Wu, 2011: A comparison of cloud radiative forcings simulated by LASG/IAP and BCC atmospheric general circulation models. *Chinese J. Atmos. Sci.*, **35**(4), 739–752. (in Chinese)

Hack, J. J., 1994: Parameterization of moist convection in the national center for atmospheric research community climate model, *J. Geophys. Res.*, **99**(D3), 5541–

5568.

Hodson, D. L. R., R. T. Sutton, C. Cassou, N. Keenlyside, Y. Okumura, and T. Zhou, 2010: Climate impacts of recent multidecadal changes in Atlantic Ocean sea surface temperature: A multimodel comparison. *Climate Dyn.*, **34**, 1041–1058.

Jackson, C. S., M. K. Sen, G. Huerta , Y. Deng, and K. P. Bowman, 2008: Error reduction and convergence in climate prediction. *J. Climate*, **21**, 6698–6709.

Kiehl, J. T., and K. E. Trenberth, 1997: Earth's annual global mean energy budget. *Bull. Amer. Meteor. Soc.*, **78**, 197–208.

Klein, S. A., and D. L. Hartmann, 1993: The seasonal cycle of low stratiform clouds. *J. Climate*, **6**, 1587–1606.

Kuang, X. Y., Y. C. Zhang, J. Liu, and L. L. Guo, 2009: A numerical study of the effect of anomalous surface heating in the Kuroshio current region in winter on the East Asian subtropical westerly jet. *Chinese J. Atmos. Sci.*, **33**(1), 81–89. (in Chinese)

Kucharski, F., and Coauthors, 2009: The CLIVAR C20C project: skill of simulating Indian monsoon rainfall on interannual to decadal timescales. Does GHG forcing play a role? *Climate Dyn.*, **33**, 615–627.

Lean, J., cited 2009: Calculations of Solar Irradiance: Monthly means from 1882 to 2008, annual means from 1610 to 2008. [Available online at http://sparcsolaris.gfzpotsdam.de/Input_data/Calculations_of_Solar_Irradiance.pdf.]

Li, L. J., and B. Wang, 2010: Influences of two convective schemes on the radiative energy budget in GAMIL1.0. *Acta Meteorologica Sinica*, **24**(3), 318–327.

Li, L. J., B. Wang, and T. J. Zhou, 2007a: Contributions of natural and anthropogenic forcings to the summer cooling over eastern China: An AGCM study. *Geophys. Res. Lett.*, **34**, L18807, doi: 10.1029/2007GL030541.

Li, L. J., B. Wang, and T. J. Zhou, 2007b: Impacts of external forcing on the 20th century global warming. *Chinese Science Bulletin*, **52**, 3148–3154.

Li, L. J., B. Wang, Y. Q. Wang, and H. Wan, 2007c: Improvements in climate simulation with modifications to the Tiedtke convective parameterization in the grid-point atmospheric model of IAP LASG (GAMIL). *Adv. Atmos. Sci.*, **24**, 323–335, doi: 10.1007/s00376-007-0323-3.

Li, L. J., Y. Q. Wang, B. Wang, and T.-J. Zhou, 2008: Sensitivity of the grid-point atmospheric model of IAP LASG (GAMIL1.1.0) climate simulations to cloud droplet effective radius and liquid water path. *Adv. Atmos. Sci.*, **25**(4), 529–540, doi: 10.1007/s00376-008-0529-z.

Li, L. J., X. Xie, B. Wang, and L. Dong, 2012: Evaluating the performances of GAMIL1.0 and GAMIL2.0 during TWP-ICE with CAPT. *Atmos. Oceanic Sci. Lett.*, **5**, 38–42.

Li, L. J., and Coauthors, 2013: The flexible global ocean-atmosphere-land system model, grid-point version 2: FGOALS-g2. *Adv. Atmos. Sci.*, doi: 10.1007/s00376-012-2140-6.

Li, J., and L. Zhang, 2009: Wind onset and withdrawal of Asian summer monsoon and their simulated performance in AMIP models. *Climate Dyn.*, **32**(7–8), 935–968.

Lin, J. L., 2007: The double-ITCZ problem in IPCC AR4 coupled GCMs: Ocean–atmosphere feedback analysis. *J. Climate*, **20**, 4497–4525, doi: http://dx.doi.org/10.1175/JCLI4272.1

Mao, J. Y., and L. J. Li, 2012: An assessment of MJO and tropical waves simulated by different versions of the GAMIL model. *Atmos. Oceanic Sci. Lett.*, **5**, 26–31.

Morrison, H., and A. Gettelman, 2008: A new two-moment bulk stratiform cloud microphysics scheme in the community atmosphere model, version 3 (CAM3). Part I: Description and numerical tests. *J. Climate*, **21**(15), 3642–3659.

Nenes, A., and J. H. Seinfeld, 2003: Parameterization of cloud droplet formation in global climate models. *J. Geophys. Res.,* **108**, 4415, doi: 10.1029/2002JD002911.

Nordeng, T. E., 1994: Extended versions of the convective parameterization scheme at ECMWF and their impact on the mean and transient activity of the model in the Tropics. ECMWF Tech. Memo. 206, 41pp.

Rasch, P. J., and J. E. Kristjánsson, 1998: A comparison of the CCM3 model climate using diagnosed and predicted condensate parameterizations. *J. Climate*, **11**(7), 1587–1614.

Sanderson, B. M., 2011: A multi-model study of parametric uncertainty in predictions of climate response to rising greenhouse gas concentrations. *J. Climate*, **24**, 1362–1377.

Scaife, A. A., and Coauthors, 2008: The CLIVAR C20C project: Selected 20th century climate events. *Climate Dyn.*, **31**, doi: 10.1007/s00382-008-0451-1.

Shi, X. J., B. Wang, X. H. Liu, M. H. Wang, L. J. Li, and L. Dong, 2010: Aerosol indirect effects on warm clouds in the grid-point atmospheric model of IAP LASG (GAMIL). *Atmos. Oceanic Sci. Lett.*, **3**, 237–241.

Stainforth, D. A., and Coauthors, 2005: Uncertainty in predictions of the climate response to rising levels of greenhouse gases. *Nature*, **433**, 403–406.

Tiedtke, M., 1989: A comprehensive mass flux scheme for cumulus parameterization in large-scale models. *Mon. Wea. Rev.*, **117**, 779–1800.

Trenberth, K. E., J. T. Fasullo, and J. Kiehl, 2009: Earth's global energy budget. *Bull. Amer. Meteor. Soc.*, **90**, 311–324.

Wang, B. and Z. Z. Ji, 2006: *New numerical methods and their applications in the atmopsheric science*. science press, 208pp.

Wang, B., H. Wan, Z. Z. Ji, X. Zhang, R. C. Yu., Y. Q. Yu, and H.-T. Liu, 2004: Design of a new dynamical core for global atmospheric models based on some efficient numerical methods. *Science in China* (*Math.*), **47**, 4–21.

Wu, Z. W., and J. Li, 2008: Prediction of the Asian-Australian monsoon interannual variations with the grid-point atmospheric model of IAP LASG (GAMIL) *Adv. Atmos. Sci.*, **25**(3), 387–394, doi: 10.1007/s00376-008-0387-8.

Wu, Z. W. and J. P. Li, 2009: Seasonal prediction of the global precipitation annual modes with the grid-point atmospheric model of IAP LASG. *Acta Meteorologica Sinica*, **23**(4), 428–437.

Xie, X., B. Wang, L.-J. Li, and L. Dong, 2012: MJO simulations by GAMIL1.0 and GAMIL2.0. *Atmos. Oceanic Sci. Lett.*, **5**, 48–54.

Xu, K. M., and S. K. Krueger, 1991: Evaluation of cloudiness parameterizations using a cumulus ensemble model. *Mon. Wea. Rev.*, **119**, 342–367.

Yan, L., P. X. Wang, Y. Q. Yu, L. J. Li, and B. Wang, 2010: Potential predictability of sea surface temperature in a coupled ocean-atmosphere GCM. *Adv. Atmos. Sci.*, **27**(4), 921–936, doi: 10.1007/s00376-009-9062-y.

Yokohata, T., M. J. Webb, M. Collins, K. D. Williams, M. Yoshimori, J. C. Hargreaves, and J. D. Annan, 2010: Structural similarities and differences in climate responses to CO_2 increase between two perturbed physics ensembles. *J. Climate*, **23**, 1392–1410.

Yu, Y., and D. Z. Sun, 2009: Response of ENSO and the mean state of the tropical Pacific to extratropical cooling and warming: a study using the IAP coupled model. *J. Climate*, **22**, 5902–5917.

Zhang, L., and J. Li, 2007: Seasonal rotation features of wind vectors and application to evaluate monsoon simulations in AMIP Models. *Climate Dyn,* doi: 10.1007/s00382-007-0327-9.

Zhang, G. J., and N. A. McFarlane, 1995: Sensitivity of climate simulations to the parameterization of cumulus convection in the Canadian climate centre general circulation model. *Atmos.–Ocean*, **33**, 407–446.

Zhang, G. J., and M. Mu, 2005: Effects of modifications to the Zhang-McFarlane convection parameterization on the simulation of the tropical precipitation in the national center for atmospheric research community climate model, version 3. *J. Geophys. Res.*, **110**, D09109, doi: 10.1029/2004JD005617.

Zheng, W. P., and Y. Q. Yu, 2009: The Asian monsoon system of the middle Holocene simulated by a coupled GCM. *Quaternary Science*, **29**, 1135–1145.

Zou, L. W., T. J. Zhou, B. Wu, H. M. Chen, and L. J. Li, 2009: The interannual variability of summertime western pacific subtropical high hindcasted by GAMIL CliPAS experiments. *Chinese J. Atmos. Sci.*, **33**, 959–970. (in Chinese)